ACES Asian Chemical Editorial Society

DOI: 10.1002/asia.201801564

CHEMISTRY
AN ASIAN JOURNAL
Full Paper

Self-Assembly

SPECIAL ISSUE

Alkylated Aromatic Thioethers with Aggregation-Induced Emission Properties—Assembly and Photophysics

Steffen Riebe,[a] Marco Saccone,[a] Jacqueline Stelzer,[a] Andrea Sowa,[a] Christoph Wölper,[c] Kateryna Soloviova,[b] Cristian A. Strassert,[b] Michael Giese,*[a] and Jens Voskuhl*[a]

Abstract: In this contribution, we present the synthesis and self-assembly of alkylated thioethers with interesting photophysical properties. To this end, the emission, absorption and excitation spectra in organic solvents and as aggregates in water were measured as well as the corresponding photoluminescence quantum yields and lifetimes. The aggregates in aqueous media were visualized and measured using transmission electron microscopy. Besides that, crystal structures of selected compounds allowed a detailed discussion of the structure–property relationship. Furthermore, the mesomorphic behavior was investigated using polarized optical microscopy (POM) as well as differential scanning calorimetry (DSC).

Introduction

The demand of organic materials which combine different properties such as highly effective and tunable emission, together with self-assembly properties yielding multi-applicable compounds is currently of high interest.[1] This approach enables an economic and efficient construction of functional materials for various purposes.[2] Especially the combination of self-assembly into larger well defined structures with particular luminescence properties is one on of the major challenges in modern materials science. One drawback of this design is that self-assembly often goes along with strong secondary interactions involving π–π stacking, besides hydrogen and halogen bonding, which leads to non-radiative charge-transfer complexes, thus quenching the fluorescence.[3] One approach to overcome this behavior is the use of a phenomenon which was first described in 2001 by the groups of Tang et al.[4] The so-called aggregation-induced emission (AIE) uses luminophores which behave contrary to classic emitters, which are typically quenched upon aggregation. Here compounds are used which exhibit a rotor like structure showing high rotational mobility in organic solvent converting absorbed light into motion, which goes along with a loss in emission. Upon aggregation a restriction of the intramolecular motion (RIM) or rotation (RIR) is obtained leading to a classic fluorophore or phosphor[5] with increased quantum yields.

Various applications of this phenomenon were described in the literature such as biomedical imaging of cell compartments,[6] photodynamic therapy,[7] luminescent micelles and vesicles,[8] organo-[9] and hydrogels[10] as well as solar cell concentrators[11] or organic light emitting diode (OLED) fabrication.[12] Nevertheless in all these applications the hindrance of intramolecular motion enhances the emission without quenching π–π interactions. In this context fluorescent liquid crystals have gained considerable attention.[13] The unique combination of intrinsic light-emission and self-organization capability makes these materials promising candidates for the application in optoelectronic devices such as light-emitting diodes and emissive liquid crystal displays.[13a,b,14]

Depending of the nature of the liquid crystalline state (e.g. nematic or cholesteric) fluorescent liquid crystals may emit linear or circular polarized light.[13b,14a,b,f,15] Another promising feature of luminescent liquid crystals is that their brightness and color can be controlled by external stimuli such as temperature or electric fields.[16] A major problem for the development of novel fluorescent liquid crystals is that typically the fluorescence emission is dramatically reduced during the formation of the ordered phase (mesophase or crystalline state).[17] However, employing AIE chromophores allows overcoming this challenge, due to the combination of an intrinsic luminescent char-

[a] S. Riebe, Dr. M. Saccone, J. Stelzer, A. Sowa, Prof. Dr. M. Giese, Prof. Dr. J. Voskuhl
Institute of Organic Chemistry, University of Duisburg-Essen
Universitätsstrasse 7, 45117, Essen (Germany)
E-mail: michael.giese@uni-due.de
jens.voskuhl@uni-due.de

[b] Dr. K. Soloviova, Prof. Dr. C. A. Strassert
Physikalisches Institut and CeNTech
Westfälische Wilhelms-Universität Münster
Mendelstrasse 7, 48149 Münster (Germany)

[c] Dr. C. Wölper
Faculty of Chemistry and Center for NanoIntegration (CENIDE)
University of Duisburg-Essen
Universitätsstrasse 5–7, 45117 Essen (Germany)

Supporting information and the ORCID identification number(s) for the author(s) of this article can be found under: https://doi.org/10.1002/asia.201801564.

This manuscript is part of a special issue on aggregation-induced emission. A link to the Table of Contents of the special issue will appear here when the complete issue is published.

acteristic, with the supramolecular organization and self-healing properties within the mesophase.[1a,18] Up to now only a few examples are known which combine the AIE phenomenon with liquid crystallinity, all based on the original approach of Tang, featuring tetraphenylethylene and diphenylacrylonitrile as core.[17,19]

Recently we were able to describe a novel class of AIE emitters based on aromatic thioethers which were easy to synthesize in high yield without costly purifications.[20] Furthermore, it was found that a simple tuning of emission wavelength can be obtained by variations of the substitution pattern as well as the introduction of different functional groups. Besides that, the self-assembly of these compounds into micelles[20b] and rods[21] as well as the application in molecular recognition of biomolecules[22] was intensively investigated. Here we describe the synthesis of alkylated AIE emitters, including a detailed investigation of the photophysical properties in different solvents, the aggregation behavior as well as a detailed structure-property relationship discussion based on X-ray diffraction analysis data. In addition, the soft crystalline properties of the materials were analyzed by polarized optical microscopy (POM) and differential scanning calorimetry (DSC).

Results and Discussion

Synthesis and photophysical properties

In a first attempt, a library of nine different compounds for the investigation of photophysical properties was synthesized. Here di-phenol derivatives were equipped with octyl-chains in a simple ether-synthesis under basic conditions leading to the desired di-alkylated compounds with different substitution patterns.

The nine compounds were categorized into *ortho*-, *meta*- and *para*-nitriles as well as *ortho*-, *meta*- and *para*-phenols with attached alkyl-chains using the abbreviations shown in Scheme 1 (e.g. *m*NP-C_8 = *meta*-nitrile *para*-phenol-C_8).

We investigated the photophysical properties of aqueous aggregate dispersions (99% water, 1% THF) at room temperature including UV/Vis, excitation and emission spectra (Figure S14-S17). All compounds appear as white to faint yellow solids, except the *para*-nitriles showing a bright yellow color.

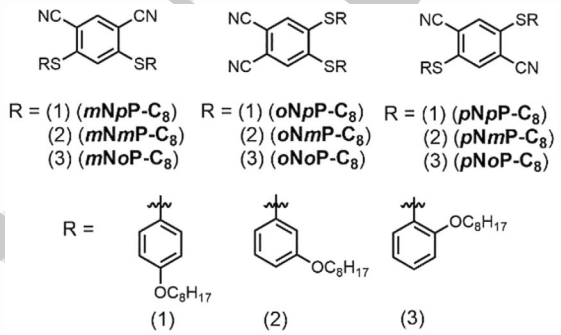

Scheme 1. Structure of the nine investigated AIE-active alkylated thioethers.

Table 1. Overview over the photophysical properties of all compounds investigated in this study.

Compound	λ_{abs} [a] ±5 [nm]	λ_{ex} [a] ±5 [nm]	λ_{em} [a] ±5 [nm]	Stokes-shift [nm/cm^{-1}]	Φ_F [a] ±1 [%]	Φ_F [b] ±1 [%]	$<\tau>$ [a,c] [ns]
***p*NpP-C$_8$**	410	405	446	36/1969	18.0	23.1	3.1
***p*NmP-C$_8$**	394	380	451	57/3208	3.6	8.8	0.9
***p*NoP-C$_8$**	389	380	451	62/3534	2.6	4.6	0.5
***o*NpP-C$_8$**	335	322	481	146/9061	5.0	7.4	1.1
***o*NmP-C$_8$**	334	322	460	126/8201	1.6	2.7	0.5
***o*NoP-C$_8$**	337	323	466	129/8214	1.6	2.6	0.3
***m*NpP-C$_8$**	290	292	457	167/12 595	4.0	5.2	1.3
***m*NmP-C$_8$**	289	301	439	150/11 823	0.9	1.4	0.6
***m*NoP-C$_8$**	302	295	439	137/10 334	1.6	1.2	0.4
***m*NpP-C$_9$**	290	295	457	167/12 601	4.2	5.5	1.0
***m*NpP-C$_{10}$**	291	295	458	167/12 530	2.1	8.3	1.0
***m*NpP-*(S)*(+)Cit**	290	294	457	167/12 601	4.0	5.1	1.1

[a] Measured for aggregates dispersions in THF/water, 1:99, average of three independent measurements. [b] Measured for solid compounds, average of three independent measurements. [c] Amplitude-weighted average lifetimes, concentration: 100 μM.

This agrees well with the absorption spectra with a broad peak centered at around 400 nm (Table 1).

Furthermore, it was found that the emission of the dispersed aggregates is strong in the blue to blue-green region of the electromagnetic spectrum (λ_{em} = 438–481 nm), depending on the substitution pattern and in good agreement with a related study.[20c]

Photoluminescence quantum yield determination (Φ_F) and lifetime measurements were also carried out for aggregates, both in the solid state and as aqueous dispersions. It was found that in general the alkyl-chains attached in *para* position lead to higher Φ_F values compared to *ortho* and *meta* within one series (e.g. *p*NpP-C_8 = 18%, *p*NmP-C_8 = 3.6% and *p*NoP-C_8 = 2.6%). We assume here a direct correlation between the packing inside the aggregates and Φ_F, which is higher ordered in the *para*-attached alkyl chains restricting the molecular motion more efficiently. Remarkably, the quantum yield of the solids is slightly higher due to a higher density and packing, compared to aqueous samples with solvent contents inside the aggregates, fixing the single compounds.

Determination of the fluorescence lifetimes (τ) reveal short-lived excited states with lifetimes below 4 ns, characteristic for fluorescence from excited singlet states (Table 1). The observed multiexponential decays are indicative of various microenvironments sensed by the emitting molecules in the aggregates, and could be related to crystal size differences or defects. (Figure S25–28).

We also investigated solvatochromic and AIE-effects. For this, we selected three compounds, one from each class (*p*NpP-C_8, *o*NpP-C_8 and *m*NpP-C_8), which were investigated concerning their emission in different THF-water mixtures (Figure 1 and S22). Interestingly all aqueous dispersions show an increased emission in the blue region with emission wavelengths below 500 nm (Table 1 and Figure S14-17). Upon undirected aggregation in poor solvents such as water, a significant

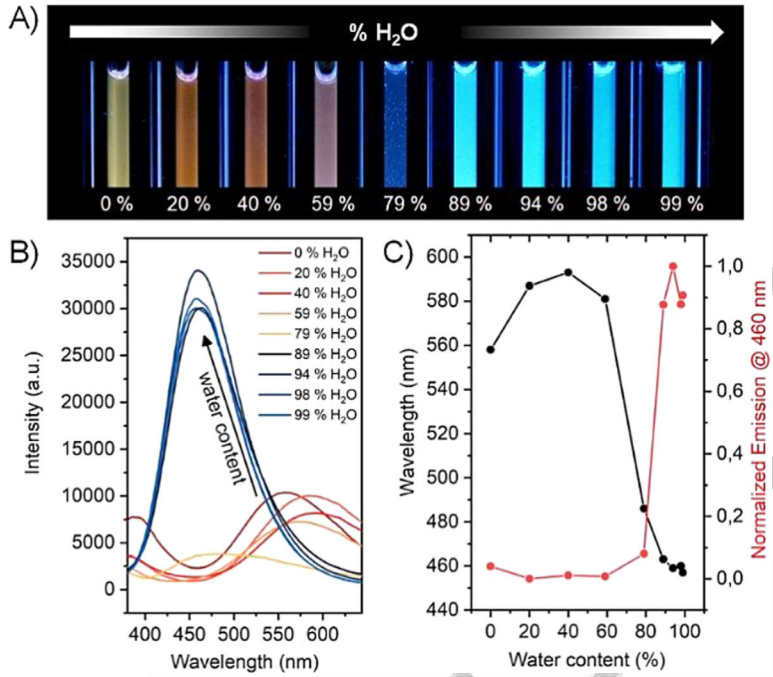

Figure 1. A) Photographs of *m*NpP-C_8 in different THF-water ratios, B) Emission spectra of the compound *m*NpP-C_8 in different THF-water ratios, C) Plot of the normalized emission intensity at 460 nm at different water contents (red) and shift in the emission maximum upon increasing water contents (black) of compound *m*NpP-C_8. Concentration: 100 μM.

hypsochromic shift is observed due to the formation of aggregates which are unable to interfere with the surrounding solvent molecules. As visible from Figure 1 the emission of the compound *m*NpP-C_8 reveals a faint yellow to red emission at high THF contents assuming a strong interaction with the surrounding solvent molecules which is lost upon fast aggregation in higher amounts of water. The undirected aggregation was found to take place at water contents higher than 79%, which is in good agreement with the hypsochromic shift overserved from Figure 1 A and C. Inside the aggregates the single compounds are hindered in their molecular freedom inducing a strong increase in emission which can be attributed to the AIE-effect.

Another remarkable finding for this compound was the high stokes shift of 167 nm (12595 cm^{-1}) which separates the excitation well from the emission wavelength.

It was found that the *para*-phenol compounds reveal a faint yellow to red emission (Figure S23) in pure THF, suggesting a positive solvatochromic effect. It indicates a strong dependence of the emission with the solvent polarity, which was confirmed by measuring the emission in solvents with different polarity. To get a deeper understanding on the solvatochromatic behavior the compounds, additional emission spectra in pure THF were recorded, revealing a bathochromic shift of the *para*-thiophenols (e.g. *p*NpP-C_8, λ_{em} = 561 nm, *m*NpP-C_8, λ_{em} = 560 nm and *o*NpP-C_8, λ_{em} = 592 nm) compared to the *meta*- and *ortho*-thiophenols (λ_{em} = 447–535 nm) (Table S1, Figure S18–21 and S23). As a representative example, emission spectra of *m*NpP-C_8, were measured in different solvents with increasing polarity (Figure S24).

These measurements confirm the expected positive solvatochromic effect with a weak green emission in toluene (relative polarity = 0.099, λ_{em} = 510 nm) and a faint red emission in acetonitrile (relative polarity = 0.460, λ_{em} = 612 nm) (Figure S24).

The aggregates formed in water were investigated in detail, to gain a deeper understanding of the morphology of the formed structures in the presence of high water contents. To this end transmission electron microscopy (TEM) was performed to visualize the emissive aggregates formed (Figure 2 and S29). As obvious from Figure 2 the selected compounds reveal small spherical aggregates in aqueous media (99%

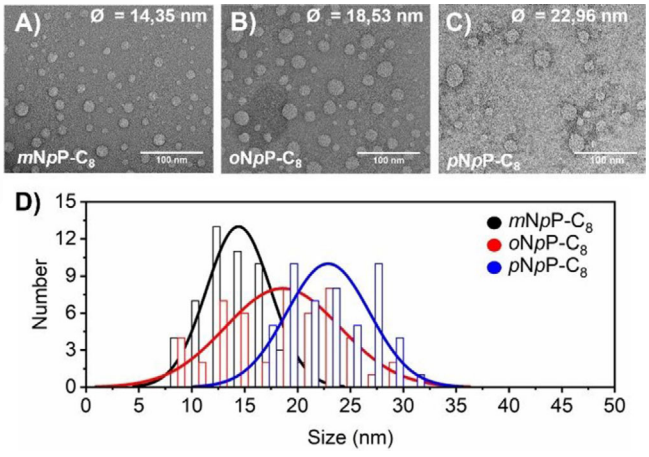

Figure 2. A) TEM image of *m*NpP-C_8, B) *o*NpP-C_8 and C) *p*NpP-C_8. D) Measured diameter distribution of the particles as obtained from TEM measurements, 50 individual particles were measured from each sample.

water, 1% THF) with averaged diameters of 15–23 nm, which is in good agreement with micellar aggregates. The differences in diameter are attributed to the different shapes of the compounds. The rod-like structure of *m*NP*p*P-C_8, facing both alkyl-chains in the same direction allows a more compact packing in the solid state. In contrast *p*NP*p*P-C_8 reveals a linear arrangement of the alkyl-chains facing in opposite directions (see Figure 5) leading to larger particles in average (see crystallographic section).

Mesomorphic Behaviour

Besides the self-assembly and photophysics in water, we also investigated the mesopmorphic behavior of the compounds by polarized optical microscopy (POM) and differential scanning calorimetry (DSC). Eight of nine compounds are solids (except *o*NO*p*P-C_8 which is an oil) with melting points between 70 and 150 °C (Table S2). To our surprise, only *m*NP*p*P-C_8 showed enantiotropic, mesomorphic behaviour, while all other compounds directly crystallized from the isotropic state (Figure S30–32). For *m*NP*p*P-C_8, this phase was observed at about 120 °C both on heating and cooling by POM (see Figure S33). Since only the substitution pattern of *m*NP*p*P-C_8 showed mesomorphic behavior, a series of compounds with alkyl chains ranging from C_8 to C_{10} as well as a chiral derivative (with a *(S)(+)*-citronellyl side chain) of *m*NP*p*P were synthesized and characterized with respect to the mesomorphic behavior (Scheme 2).

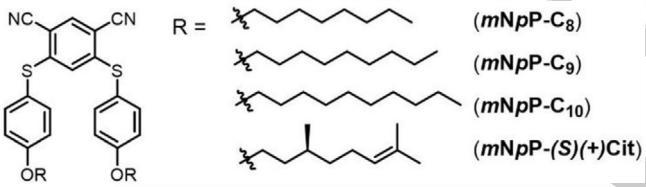

Scheme 2. Second generation library with varying alkylchains.

We noticed several interesting features of these assemblies. First, enantiotropic mesomorphism was only observed for linear alkyl chains with even numbers of carbon atoms (C_8 and C_{10}), while *(S)(+)*-Cit and C_9 only displayed monotropic soft-crystalline behavior; second, this phase is displayed by the *m*NP*p*P-C_n compounds. The following discussion will focus on the results obtained *m*NP*p*P-C_{10} as a representative example.

POM results were confirmed by DSC (Figure 3 D–E) which showed in the case of *m*NP*p*P-C_{10} the presence of two endothermic transitions on heating, and two exothermic and a glass transition upon cooling. The transition energy is high for the transition into the isotropic phase (18.2 $J g^{-1}$ and 17.8 $J g^{-1}$), indicating strong structural changes at these transitions, and small for the remaining transitions (−0.3 $J g^{-1}$ and −0.15 $J g^{-1}$, the latter for the glass transition), thus indicating minor structural changes.

A very similar behaviour is shown by its C_8 analogue, while the other two (C_9 and *(S)*Cit) did not show any other transition

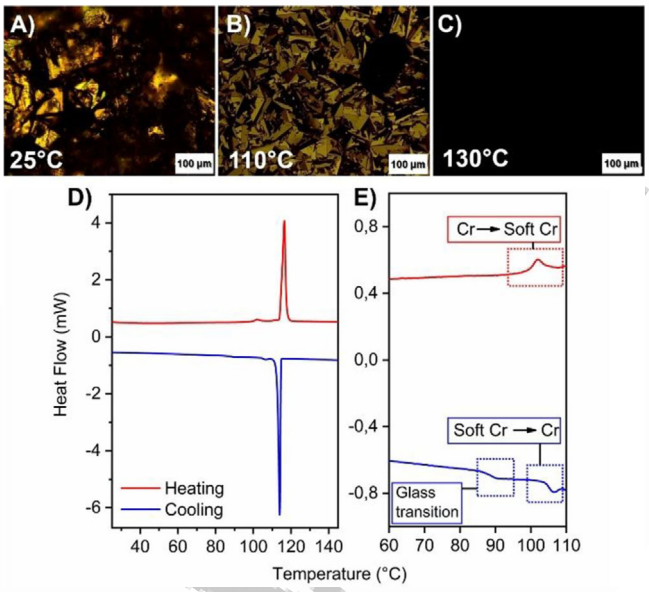

Figure 3. Top, representative POM pictures of mNpP-C10 in the crystalline (A), soft crystalline (B), and isotropic (C) state at different temperatures. In all the pictures, polarizers are crossed. Bottom, DSC trace of mNpP-C10 (D) in. (E) represents a magnified view of (D) in which the relevant transitions are highlighted.

apart from the melting and the crystallization (Figure S34, Table S3).

In addition, the fluorescence behaviour of *m*NP*p*P-C_{10} was studied by optical microscopy upon cooling. Therefore, the sample was heated to 125 °C and irradiated with 360 nm. Since the sample is in its isotropic state at this temperature and the sample was observed without polarizers, no specific texture and fluorescence was observed (Figure 4 A).

Upon cooling to 110 °C, however, fluorescent regions slowly emerged (Figure 4 B and C), which are highly birefringent when observed under crossed polarizers (Figure 4 D). These

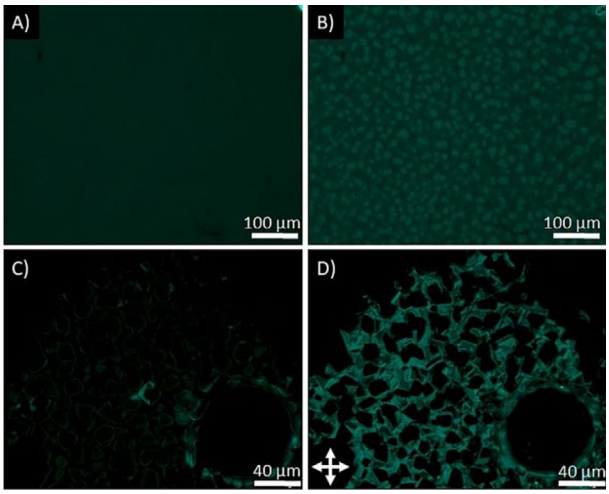

Figure 4. Fluorescence micrographs of *m*NP*p*P-C_{10} under UV excitation (360 nm) upon cooling from the isotropic state (125 °C, A). Fluorescent regions emerged starting at 110 °C (B and C), which are birefringent under crossed polarizers (D).

textures are indicative for the formation of highly ordered phase/mesophase, which restricts the free rotation of the phenyl-units and thereby enables the AIE effect.

X-ray structure determination

To get a deeper insight in the correlation between the material properties and the molecular structures of the compounds, X-ray diffractometric analysis of single crystals was performed (Figure S35–42). To this end, three structures were investigated in detail (Figure 5) and discussed concerning their secondary

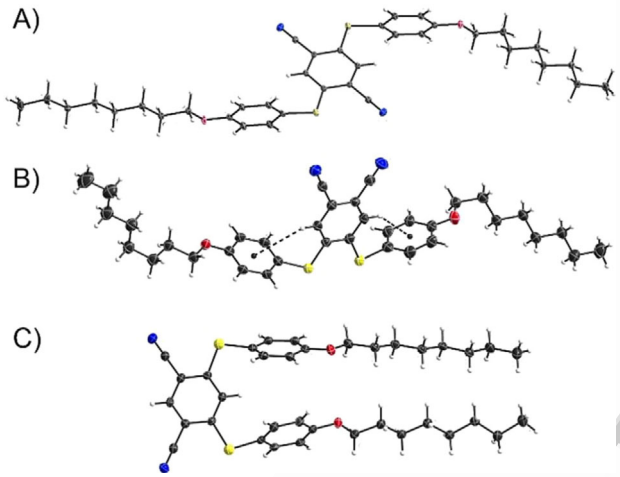

Figure 5. Molecular structures as obtained by X-ray diffractometric analysis of single crystals of *m*N*p*P-C_8 (A) *o*N*p*P-C_8 (B) and *p*N*p*P-C_8 (C).

interactions as well as orientations in the crystal lattice. *m*N*p*P-C_8 shows a hairpin-like conformation (Figure S35, Figure 5). There are no apparent intra-molecular interactions that stabilize this orientation of the residual groups. The inter-planar angle of the phenyl rings is too large (47.05°) to support meaningful π···π interactions. The packing is constituted mainly by two motifs. The first one connects the residual groups' phenyl rings with S and N atoms of a molecule related by the c glide plane (Figure 6).

These interactions reduce the rotational freedom of the residual groups, which explains the induced fluorescence. Since any atom of the alkyl chains can be donor for a non-classical hydrogen bond to form a similar motif, it is likely that the molecules can be shifted along its axis without substantially destabilizing the packing. This causes the soft crystalline properties. In the crystalline phase, the most acidic CH donor, that is, phenyl C–H, forms the hydrogen bond. The second is a non-classical hydrogen bond from the central phenyl ring to the nitrile- nitrogen. (Figure 7)

This yields a layer with the alkyl chains on both sides. The dents in the layer's surface are filled with alkyl chains of the neighboring layer. As a result, all molecules are oriented approximately parallel to [203].

The molecules of *p*N*p*P-C_8 are not centrosymmetric. The different conformation of the alkyl chains hampers the symmetry.

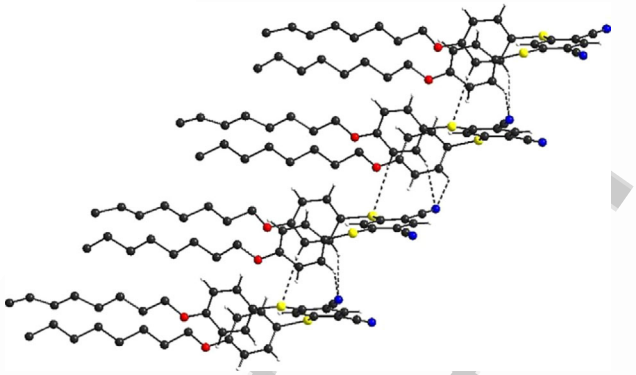

Figure 6. Representative view of the crystal lattice in *m*N*p*P-C_8 including interactions between the phenyl rings with the N and S atoms of a molecule related by the *c* glide plane forcing the restriction of intramolecular rotation.

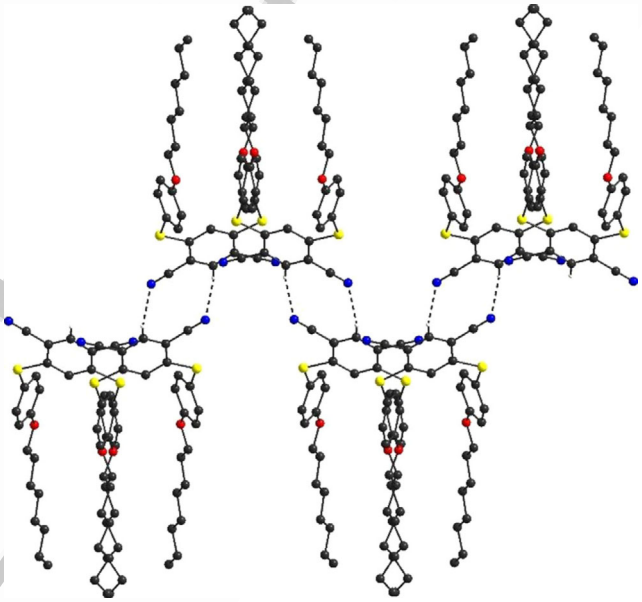

Figure 7. Representative view of the packing inside the crystal lattice of *m*N*p*P-C_8, revealing a linear orientation of the alkyl chains and a non-classical hydrogen bond from the central phenyl ring the nitrile nitrogen.

The O2-C29-C30-C31 torsion angle of approx. 60° leads to a "bent" conformation of one alkyl chain while the other residue is "straight" with all O/C–C–C–C torsion angles roughly 180° (Figure 5 and S40). All hydrogen atoms of the S-Ph groups are involved in non-classical hydrogen bonding (see Table S6) and are connected to the neighboring molecule related by translational symmetry which yields a layer parallel to (001) (Figure 8).

These layer are connected on one side by C–H···π interactions and non-classical hydrogen bonds involving the nitrile group and the neighboring proton of the ring. This pattern is also found in *m*N*p*P-C_8 (see Figure 7). The proximity of the nitrile groups is only possible because the "straight" alkyl chains can penetrate the neighboring layer (Figure S42).

On the opposite side of the layer the "bent" alkyl chains' ends form a C–H···π interaction with the phenyl ring of the inverted arm and the formation of dimeric species. All inter-layer interactions are generated via inversion symmetry. Due to this

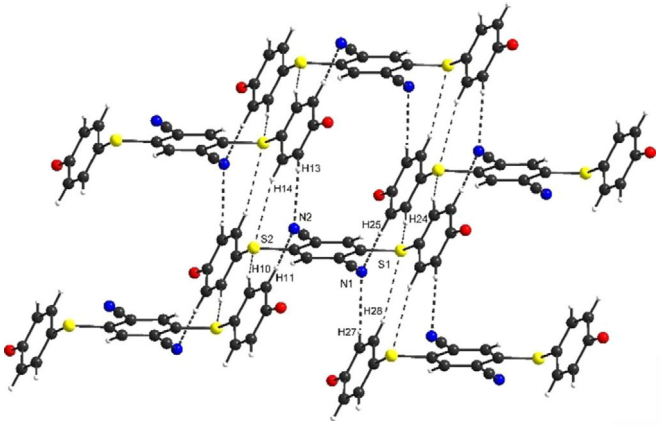

Figure 8. Packing of *p*N*p*P-C_8 in the crystal lattice including inter- and intra-molecular interactions, alkyl chains are omitted for clarity.

dense network the motional freedom is restricted, which explains the higher PLQY (Φ_F (solid) = 23.1%, Φ_F (aggregate) = 18.0%) compared to *m*N*p*P-C_8 (Φ_F (solid) = 5.0%, Φ_F (aggregate) = 4.2%). Furthermore, a shifting along a specific axis is dramatically hindered (see compound *m*N*p*P-C_8) leading to a pure crystalline behavior upon cooling without any mesophase.

The overall linear conformation of *o*N*p*P-C_8 likely results from two intra-molecular CH···π interaction between the hydrogen atoms of the central ring and the π-systems of the side arms' phenyl rings (Figure 9 and S44). These limit the motional

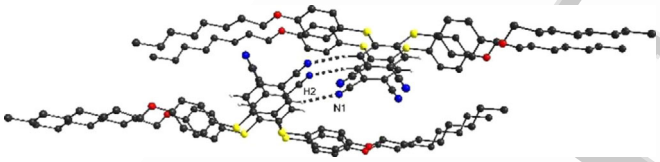

Figure 9. Packing of *o*N*p*P-C_8 in the crystal lattice including intermolecular interactions.

and rotational freedom of the side-arms which is beneficial for the induced fluorescence compared to *m*N*p*P-C_8 (*m*N*p*P-C_8 (Φ_F (solid) = 5.0%, Φ_F (aggregate) = 4.2%, *o*N*p*P-C_8 (Φ_F (solid) = 7.4%, Φ_F (aggregate) = 5.0%). The conformation of the alkyl chains slightly differ which can be attributed to the formation of a close packing hindering a gliding between single planes, which is in good agreement with the pure crystalline behavior. The molecules are lined up along the 2_1 axis and connected by a non-classical hydrogen bond (see Figure 9, same motif in *m*N*p*P-C_8 Figure 7). This alignment leads to short contacts between the nitrogen atoms and phenyl π-systems.

Conclusions

To conclude, we described a unique system based on alkylated thioethers with interesting photophysical properties. The observed aggregation-induced emission (AIE) was assessed using techniques such as fluorescence spectroscopy, determination of the photoluminescence quantum yields as well as the excited state lifetimes. The aggregates were studied using transmission electron microscopy, leading to a direct correlation between the shape of the compounds and the size of the aggregates. The detailed investigation of all compounds concerning their mesomorphic behavior showed that linearly arranged alkylated thioethers (*m*N*p*P-C_n) with even numbers of carbon atoms gave an enantiotropic mesomorphism with soft crystalline behavior. Interestingly, branched alkyl chains (*m*N*p*P-(*S*)(+)-Cit) or odd numbered (C_9) alkyl-chains showed monotopic transition. This behavior was correlated with the molecular structures obtained for *m*N*p*P-C_8 revealing a gliding plane necessary for the soft crystallinity, which is not present for all the other *meta*-, *ortho*- and *para*- compounds. The investigation of the induced emission during the cooling process from the isotropic phase and the formation of the soft crystalline phase was performed by combined POM and fluorescence microscopy revealing the appearance of birefringent structures. In an upcoming study we will investigate in detail the origin of the soft crystallinity in relation to the molecular structures using a novel combined theoretical and experimental approach.

Acknowledgements

We acknowledge the support of the Interdisciplinary Center for Analytics on the Nanoscale (ICAN Duisburg, Germany) for providing the transmission electron microscope used in this work. Jun.-Prof. Jens Voskuhl, Jun.-Prof. Michael Giese and Jacqueline Stelzer acknowledge the Fonds der Chemischen Industrie and the Center for Nanointergation (CENIDE) for financial support. Jun.-Prof. Michael Giese is thankful for generous financial support by the Professor Werdelmann Stiftung. Jörg Rust and Christian W. Lehmann and the Petra III Beamline P11 at DESY are acknowledged for the determination of the X-ray structure of compound *p*N*p*P-C_8 (CCDC: 1871602). Dr. Constantin G. Danilliuc is acknowledged for the determination of the X-ray structure *m*N*p*P-C_8 and *o*N*p*P-C_8 (CCDC: 1871491 and 1877494). Jan Balszuweit is acknowledged for the help during the determination of the photoluminescence quantum yields and the fluorescence lifetimes. Dr. Kateryna Soloviova acknowledges the Alexander-von-Humboldt-Foundation for a postdoctoral fellowship.

Conflict of interest

The authors declare no conflict of interest.

Keywords: aggregation-induced emission · fluorescence · mesomorphism · self-assembly · X-ray diffractometric analysis

[1] a) J. Mei, N. L. C. Leung, R. T. K. Kwok, J. W. Y. Lam, B. Z. Tang, *Chem. Rev.* **2015**, *115*, 11718 – 11940; b) Y. Hong, J. W. Y. Lam, B. Z. Tang, *Chem. Soc. Rev.* **2011**, *40*, 5361 – 5388.
[2] J. Mei, Y. Hong, J. W. Y. Lam, A. Qin, Y. Tang, B. Z. Tang, *Adv. Mater.* **2014**, *26*, 5429 – 5479.
[3] C. R. Martinez, B. L. Iverson, *Chem. Sci.* **2012**, *3*, 2191 – 2201.
[4] J. Luo, Z. Xie, J. W. Y. Lam, L. Cheng, H. Chen, C. Qiu, H. S. Kwok, X. Zhan, Y. Liu, D. Zhu, B. Z. Tang, *Chem. Commun.* **2001**, 1740 – 1741.

[5] M. Hayduk, S. Riebe, J. Voskuhl, *Chem. Eur. J.* **2018**, *24*, 12221 – 12230.
[6] a) C. Y.-W. Lo, S. Chen, S. J. Creed, M. Kang, N. Zhao, B. Z. Tang, K. D. Elgass, *Sci. Rep.* **2016**, *6*, 30855; b) X. L. Cai, F. Hu, G. X. Feng, R. T. K. Kwok, B. Liu, B. Z. Tang, *Isr. J. Chem.* **2018**, *58*, 860 – 873.
[7] a) N. Alifu, X. Dong, D. Li, X. Sun, A. Zebibula, D. Zhang, G. Zhang, J. Qian, *Mater. Chem. Front.* **2017**, *1*, 1746 – 1753; b) C.-C. Chang, M.-C. Hsieh, J.-C. Lin, T.-C. Chang, *Biomaterials* **2012**, *33*, 897 – 906; c) B. Gu, W. Wu, G. Xu, G. Feng, F. Yin, P. H. J. Chong, J. Qu, K. T. Yong, B. Liu, *Adv. Mater.* **2017**, *29*, 1701076.
[8] a) M. Zhang, X. Yin, T. Tian, Y. Liang, W. Li, Y. Lan, J. Li, M. Zhou, Y. Ju, G. Li, *Chem. Commun.* **2015**, *51*, 10210 – 10213; b) N. Zhang, H. Chen, Y. Fan, L. Zhou, S. Trépout, J. Guo, M.-H. Li, *ACS Nano* **2018**, *12*, 4025 – 4035.
[9] M. Externbrink, S. Riebe, C. Schmuck, J. Voskuhl, *Soft Matter* **2018**, *14*, 6166 – 6170 ■■ok as changed?■■.
[10] C. Zhang, C. Liu, X. Xue, X. Zhang, S. Huo, Y. Jiang, W.-Q. Chen, G. Zou, X.-J. Liang, *ACS Appl. Mater. Interfaces* **2014**, *6*, 757 – 762.
[11] A. Pucci, *Isr. J. Chem.* **2018**, *58*, 837 – 844.
[12] F. Rizzo, F. Cucinotta, *Isr. J. Chem.* **2018**, *58*, 874 – 888.
[13] a) G. Lüssem, J. H. Wendorff, *Polym. Adv. Technol.* **1998**, *9*, 443 – 460; b) K. S. Whitehead, M. Grell, D. D. C. Bradley, M. Inbasekaran, E. P. Woo, *Synth. Met.* **2000**, *111 – 112*, 181 – 185; c) J. Seo, S. Kim, S. H. Gihm, C. R. Park, S. Y. Park, *J. Mater. Chem.* **2007**, *17*, 5052 – 5057; d) R. K. Vijayaraghavan, S. Abraham, H. Akiyama, S. Furumi, N. Tamaoki, S. Das, *Adv. Funct. Mater.* **2008**, *18*, 2510 – 2517; e) Y. Sagara, T. Kato, *Angew. Chem. Int. Ed.* **2008**, *47*, 5175 – 5178; *Angew. Chem.* **2008**, *120*, 5253 – 5256; f) C. V. Yelamaggad, A. S. Achalkumar, D. S. S. Rao, S. K. Prasad, *J. Org. Chem.* **2009**, *74*, 3168 – 3171; g) V. de Halleux, J.-P. Calbert, P. Brocorens, J. Cornil, J.-P. Declercq, J.-L. Brédas, Y. Geerts, *Adv. Funct. Mater.* **2004**, *14*, 649 – 659; h) T. Yasuda, H. Ooi, J. Morita, Y. Akama, K. Minoura, M. Funahashi, T. Shimomura, T. Kato, *Adv. Funct. Mater.* **2009**, *19*, 411 – 419.
[14] a) B. A. San Jose, S. Matsushita, Y. Moroishi, K. Akagi, *Macromolecules* **2011**, *44*, 6288 – 6302; b) H. Hayasaka, T. Miyashita, K. Tamura, K. Akagi, *Adv. Funct. Mater.* **2010**, *20*, 1243 – 1250; c) H. Hayasaka, K. Tamura, K. Akagi, *Macromolecules* **2008**, *41*, 2341 – 2346; d) M. Grell, D. D. C. Bradley, *Adv. Mater.* **1999**, *11*, 895 – 905; e) A. Beer, G. Scherowsky, H. Owen, H. Coles, *Liq. Cryst.* **1995**, *19*, 565 – 572; f) T. Christ, A. Greiner, R. Sander, V. Stümpflen, J. H. Wendorff, *Adv. Mater.* **1997**, *9*, 219 – 222.
[15] Y. S. Jeong, K. Akagi, *J. Mater. Chem.* **2011**, *21*, 10472 – 10481.
[16] Y. Sagara, S. Yamane, T. Mutai, K. Araki, T. Kato, *Adv. Funct. Mater.* **2009**, *19*, 1869 – 1875.
[17] S. Jiang, J. Qiu, Y. Chen, H. Guo, F. Yang, *Dyes Pigm.* **2018**, *159*, 533 – 541.
[18] J. Kim, S. Cho, B.-K. Cho, *Chem. Eur. J.* **2014**, *20*, 12734 – 12739.
[19] H. T. Bui, J. Kim, H.-J. Kim, B.-K. Cho, S. Cho, *J. Phys. Chem. C* **2016**, *120*, 26695 – 26702.
[20] a) S. Riebe, C. Vallet, F. v. d. Vight, D. Gonazles-Abradelo, C. Wölper, C. A. Strassert, G. Jansen, S. Knauer, J. Voskuhl, *Chem. Eur. J.* **2017**, *23*, 13660 – 13668; b) B. Schmidt, S. Sankaran, L. Stegemann, C. A. Strassert, P. Jonkheijm, J. Voskuhl, *J. Mater. Chem. B* **2016**, *4*, 4732 – 4738; c) J. Stelzer, C. Vallet, A. Sowa, D. Gonzalez-Abradelo, S. Riebe, C. G. Daniliuc, M. Ehlers, C. A. Strassert, S. K. Knauer, J. Voskuhl, *ChemistrySelect* **2018**, *3*, 985 – 991.
[21] H. Frisch, D. Spitzer, M. Haase, T. Basché, J. Voskuhl, P. Besenius, *Org. Biomol. Chem.* **2016**, *14*, 5574 – 5579.
[22] M. Hayduk, S. Riebe, K. Rudolph, S. Schwarze, F. van der Vight, C. G. Daniliuc, G. Jansen, J. Voskuhl, *Isr. J. Chem.* **2018**, *58*, 927 – 931.

Manuscript received: October 24, 2018
Revised manuscript received: November 7, 2018
Accepted manuscript online: ■■ ■■, 0000
Version of record online: ■■ ■■, 0000

FULL PAPER

Self-Assembly

Steffen Riebe, Marco Saccone, Jacqueline Stelzer, Andrea Sowa, Christoph Wölper, Kateryna Soloviova, Cristian A. Strassert, Michael Giese, Jens Voskuhl**

■■ – ■■

Alkylated Aromatic Thioethers with Aggregation-Induced Emission Properties—Assembly and Photophysics

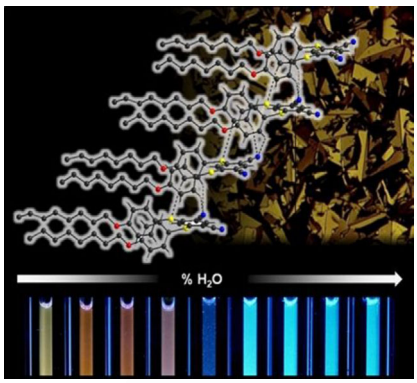

Shiny and soft: A series of alkylated aromatic thioethers were synthesized and thoroughly investigated with regard to their photophysical properties, their self-assembly behavior as well as their formation of soft crystals. Furthermore, the structure–property relationship was studied in detail.

Michael Giese, Jens Voskuhl and co-workers @unidue report on the synthesis & self-assembly of alkylated #thioethers with aggregation-induced rmission properties SPACE RESERVED FOR IMAGE AND LINK

Share your work on social media! *Chemistry – An Asian Journal* has added Twitter as a means to promote your article. Twitter is an online microblogging service that enables its users to send and read short messages and media, known as tweets. Please check the pre-written tweet in the galley proofs for accuracy. If you, your team, or institution have a Twitter account, please include its handle @username. Please use hashtags only for the most important keywords, such as #catalysis, #nanoparticles, or #proteindesign. The ToC picture and a link to your article will be added automatically, so the **tweet text must not exceed 250 characters**. This tweet will be posted on the journal's Twitter account (follow us @ChemAsianJ) upon publication of your article in its final (possibly unpaginated) form. We recommend you to re-tweet it to alert more researchers about your publication, or to point it out to your institution's social media team.

Please check that the ORCID identifiers listed below are correct. We encourage all authors to provide an ORCID identifier for each coauthor. ORCID is a registry that provides researchers with a unique digital identifier. Some funding agencies recommend or even require the inclusion of ORCID IDs in all published articles, and authors should consult their funding agency guidelines for details. Registration is easy and free; for further information, see http://orcid.org/.

Steffen Riebe
Dr. Marco Saccone
Jacqueline Stelzer
Andrea Sowa
Dr. Christoph Wölper
Dr. Kateryna Soloviova
Prof. Dr. Cristian A. Strassert
Prof. Dr. Michael Giese
Prof. Dr. Jens Voskuhl http://orcid.org/0000-0002-9612-2306